Archives of Civil and Mechanical Engineering (2023) 23:109
https://doi.org/10.1007/s43452-023-00652-4

ORIGINAL ARTICLE

Probabilistic finite element analysis of failures in concrete dams with large asperities in the rock–concrete interface

Adrian Ulfberg[1] · Jaime Gonzalez-Libreros[1] · Oisik Das[1] · Dipen Bista[2,3] · Marie Westberg Wilde[4,5] · Fredrik Johansson[4] · Gabriel Sas[1]

Received: 9 February 2023 / Revised: 15 March 2023 / Accepted: 26 March 2023 / Published online: 8 April 2023

Abstract
Common analytical assessment methods for concrete dams are unlikely to predict material fracture in the dam body because of the assumption of rigid body behavior and uniform- or linear stress distribution along a predetermined failure surface. Hence, probabilistic non-linear finite element analysis, calibrated from scale model tests, was implemented in this study to investigate the impact of concrete material parameters (modulus of elasticity, tensile strength, compressive strength, fracture energy) on the ultimate capacity of scaled model dams. The investigated dam section has two types of large asperities, located near the downstream and/or upstream end of the rock–concrete interface. These large-scale asperities significantly increased the interface roughness. Post-processing of the numerical simulations showed interlocking between the buttress and the downstream asperity leading to fracture of the buttress with the capacity being determined mainly by the tensile strength of the buttress material. The capacity of a model with an asperity near the upstream side, with lower inclination, was less dependent on the material parameters of the buttress as failure occurred by sliding along the interface, even with inferior material parameters. Results of this study show that material parameters of the concrete in a dam body can govern the load capacity of the dam granted that significant geometrical variations in the rock–concrete interface exists. The material parameters of the dam body and their impact on the capacity with respect to the failure mechanism that developed for some of the studied models are not commonly considered to be decisive for the load capacity. Also, no analytical assessment method for this type of failure exists. This implies that common assessment methods may misjudge the capacity and important parameters for certain failure types that may develop in dams.

Keywords Concrete dams · Model test · Numerical analysis · Material randomization · Probabilistic finite element modeling · Dam failure

1 Introduction

Structural assessment of concrete dams usually involves evaluation of three separate failure modes: overturning, sliding, and overstressing [1–3]. Although the mentioned failure modes are complex, they are often evaluated using analytical methods based on rigid body analyses, thereby reducing the problems to mere summation of the stabilizing and destabilizing moments and forces. These models are easy to apply and are often recommended by governing standards and guidelines [1, 2, 4–7]. However, they involve substantial simplification, for example, the assumption of constant normal stress in the interface for the sliding failure mode and disregard the presence of any large asperities in the rock–concrete interface between the dam and its foundation.

Such idealizations of the rock–concrete interface can be conservative with regards to the capacity associated with the respective failure modes as shown by previous studies [8–11], which allude at a significant contribution from macro-asperities on the capacity of sheared interfaces.

✉ Gabriel Sas
gabriel.sas@ltu.se

1 Department of Civil, Environmental and Natural Resources Engineering, Luleå University of Technology, Laboratorievägen 14, 971 87 Luleå, Sweden

2 Norwegian University of Science and Technology, Trondheim, Norway

3 SINTEF Narvik, Narvik, Norway

4 Division of Soil- and Rock Mechanics, KTH Royal Institute of Technology, Stockholm, Sweden

5 AFRY, Stockholm, Sweden

While many shear strength criteria include the influence of interface roughness [8, 12–18], some are not applicable for large-scale asperities or give an unreasonably low shear strength when applied to large asperity sizes [19]. Hencher and Richards [20] proposed a method for estimating the shear strength, which allows for the inclusion of large-scale asperities by adjustment of the friction angle. While the contribution of the large-scale asperities can be accounted for in this analytical model, failure is assumed to occur by sliding over the large scale asperities. This type of failure can be governing for interfaces where the asperities have a low inclination with respect to the plane of sliding. However, for large-scale asperities with high inclination, failure is more likely to occur in the asperity [21, 22]. The critical angle at which the failure occurs in the asperity may also depend on the rock type [15]. Furthermore, in a study regarding the location of large-scale asperities along eccentrically loaded interfaces, like those of dam structures, Bista et al. [23] found that the shear capacity of such interfaces varied greatly depending on the large asperities' positions along the interface. This effect is not replicable with any of the mentioned shear strength criteria.

To counter shortcomings of the analytical methods outlined above, other evaluation methods such as scale model testing or numerical analysis can be utilized. Scale model testing is a well-established analysis method in structural engineering [24] and has been used extensively in analyses of dam structures [25–29]. It allows inclusion of the geometry of the interface without exaggerated idealization and accounts for any non-uniform stress distributions in the interface. However, a scale model is only representative of the prototype (real structure) if it fulfills similitude requirements [24]. For example, it may be difficult to reproduce a certain concrete's inelastic behavior fully in a scale model, resulting in distortions of the results [24]. In finite element analysis (FEA) there is no such problem, and the structure can be represented at any scale without any associated financial or practical constraints. Results from finite element (FE) models should be carefully considered due to uncertainties regarding the correctness of their representation of real structures, but results from scale model tests can be used to benchmark and calibrate the models, thereby increasing their trustworthiness [30].

FEA can also be used in conjunction with probabilistic analysis, which enables assessment of the effects of changes in parameters (e.g., materials' strength variables) on structures' capacities and responses [31]. It also enables for a sensitivity analysis, which provides insights regarding the most influential parameters [31]. Probabilistic finite element analysis (PFEA) can potentially improve dam stability calculations, by systematically addressing randomness in geometry or materials.

The aim of this study is to show how probabilistic finite element methods can be used to predict complex failure mechanism in concrete dams. Being able to determine the variables governing the capacity and failure mode of a dam more accurately would not only lead to material savings in new structures but also improve the assessment of existing ones and therefore avoid unnecessary strengthening actions or replacement. Very few studies of this type have been done, and thus the method presented here together with the results will benefit both the research and engineering community in analysing stability of dams with more confidence. Many studies have focused on investigating the effects of small asperities and roughness along the shearing plane [13, 14, 32]. However, studies on how large-scale variations of the rock–concrete interface and how to account for them in assessment, to the best knowledge of the authors, have not been reported.

The study focused on the effects of concrete mechanical properties on capacities and failure modes of dams with varying rock–concrete interface geometries by applying PFEA to data obtained in previous scale model tests [19]. The models include four parameters of the concrete material in the dam buttress as random variables: the modulus of elasticity, tensile strength, compressive strength, and fracture energy. After presenting the tests, models and results, the parameters' influences on capacity and failure mode are discussed for each simulated scale model.

2 Scale model tests

Sas et al. [19] investigated effects of large-scale asperities on the capacity of a buttress dam section through scale model tests and FEA simulations. As described in detail by the cited authors, the scale models' prototype (real structure) is a section of Kalhovd dam, an existing 386 m long buttress dam in Norway with buttress heights varying between 1.5 and 13.3 m [19]. A recent assessment by deterministic analytical methods concluded that it had an unsatisfactory safety factor according to relevant standards [6]. Distinguishing features of this dam section that make it highly appropriate for this study are two large asperities along the interface between the dam and rock foundation, referred to as the rock–concrete interface [19]. These two large scale-asperities were neglected in the deterministic analytical assessment and the rock–concrete interface was assumed to be flat. The real dam section is depicted in Fig. 1.

Four scale models were created from the prototype shown in Fig. 1. They differed geometrically as one model included both large asperities (equivalent to the real geometry of the rock–concrete interface), two included only one of the asperities, either the upstream or the downstream asperity, and one did not include any asperities and instead had a

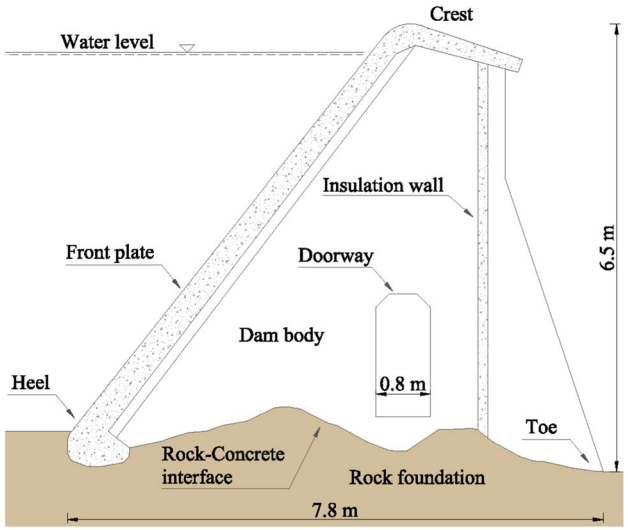

Fig. 1 Prototype buttress dam section used in scale model tests conducted by Sas et al. [19], reproduced under the terms of the Creative Commons Attribution (CC BY 4.0) license

flat interface geometry (equivalent to the idealized geometry used in the analytical assessments). They were named according to whether they included the upstream asperity (UA), downstream asperity (DA), both asperities (UDA) or neither asperity (R, the reference model). The rock–concrete interfaces of the scale models that included one or more asperities are depicted in Fig. 2.

The models were produced with a scale of 1:5 using similitude theory [33], where similarity criteria were enforced on loads, geometry, and material properties. The front plate and the insulation wall of the existing prototype were not included in the scale models, only the buttress wall of the dam section. This is justified by Sas et al. [19] by mentioning that the only geometrical difference between the models is the rock–concrete interface. Only the buttress wall (hereby referred to only as buttress) was subjected to the scaling. This implies that material properties of the foundations of the individual buttresses were ignored in the scaling process and they were instead cast from C30/37 concrete, conforming to the relevant Eurocode [34]. To obtain the material parameters required by the scaling laws, the buttress had to

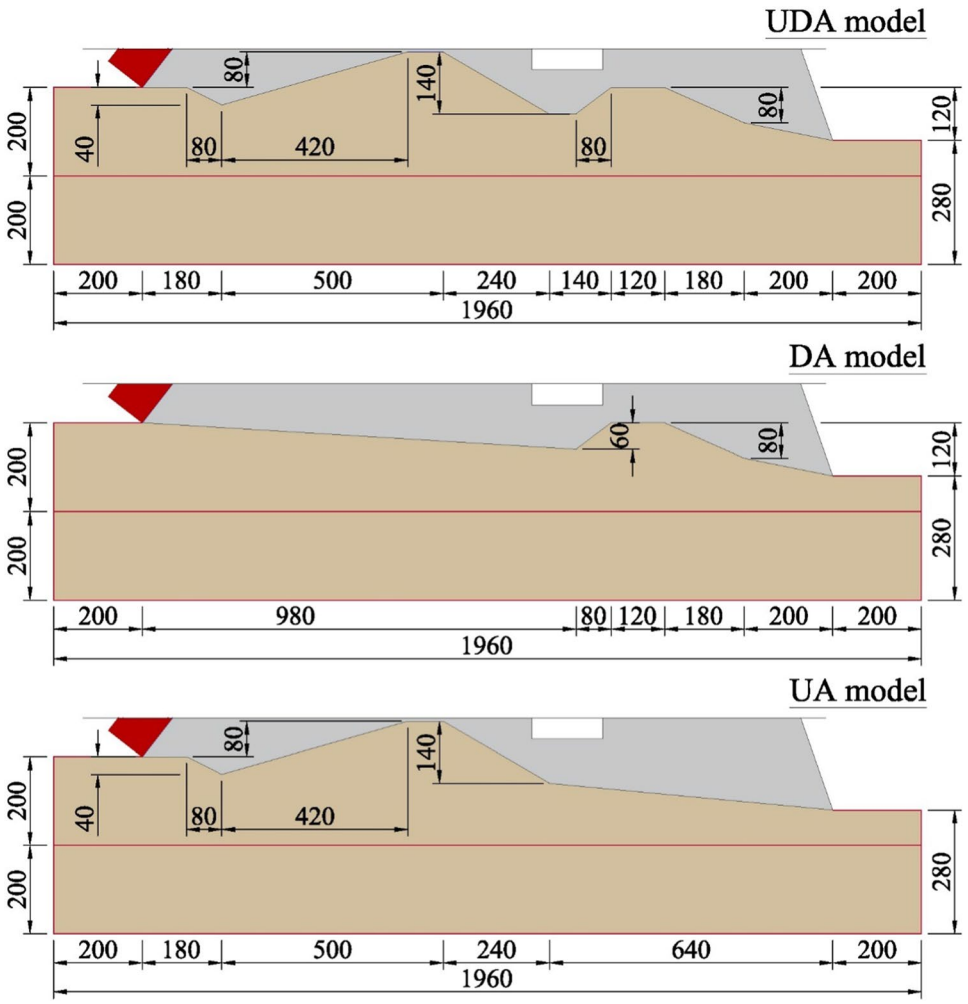

Fig. 2 Rock–concrete interfaces (units in [mm]) of the three scale models by Sas et al. [19], reproduced under the terms of the Creative Commons Attribution (CC BY 4.0) license

be cast from mortar. The buttress mortar mix consisted of 1 part cement, 0.6 parts water and 3 parts sand with aggregate sizes 0–4 mm [19]. From each buttress model mortar mix, cylinders and cubes were cast to obtain the material properties. Tilt angle tests on cubes were used to determine the basic friction angle [19].

The test setup (named sliding loading scheme) is shown in Fig. 3. It consisted of two hydraulic jacks, P1 and P2, pushing on a loading beam (HEA 100) to provide a triangular distribution of the load (equivalent to that of hydrostatic pressure). The hydraulic jacks P1 and P2 applied 55% and 45% of the total applied force, respectively. They were controlled by servo valves and programmed to apply a linearly increasing load, with a load rate of 2.4 kN/min for both jacks during the duration of the test [19]. A guiding system was implemented to keep the buttress in its plane as the scale model did not include the front plate. The foundation of the buttress was anchored to a thick concrete floor to prevent it from sliding [19].

The governing failure mode for all the scale models should have been, according to the common analytical assessment methods, sliding failure along the rock–concrete interface. However, the DA and UDA scale models failed by rupture in the buttress, diagonally from the front asperity in the UDA scale model and from the back asperity in the DA scale model. This implies that overstressing of the buttress material occurred rather than interface sliding. Only the reference scale model (R) and UA scale model failed by sliding along the rock–concrete interface [19]. During the tests the models were monitored by digital image correlation (DIC), a non-contact photogrammetric technique to measure surface deformations in 2D or 3D. The DIC strain measurements were used for comparisons with the FEA models, as described in Sect. 5.

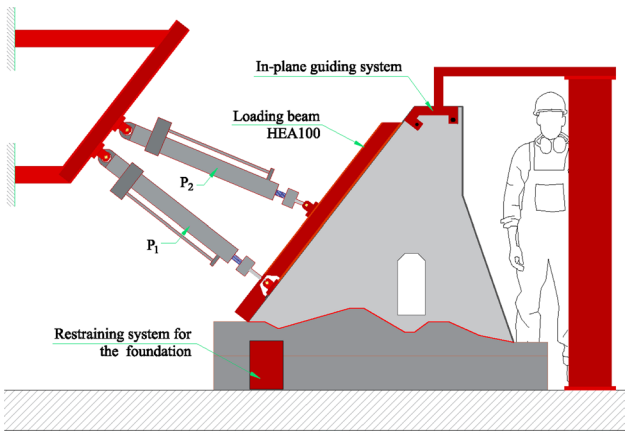

Fig. 3 Test setup for the sliding tests performed by Sas et al. [19], reproduced under the terms of the Creative Commons Attribution (CC BY 4.0) license

With capacities of the structures estimated with the Mohr–Coloumb failure criterion, and assumption that the failure plane was flat between the extreme points in the toe and heel of the specimens, the load representing the water pressure at which sliding failure of the scale models would occur was 2.2–2.7 kN. The specified range is due to the variability in the measured basic friction angles from the tilt angle tests. The R and UA scale model failed in the experimental tests by sliding, but at a total applied load of 4.4 kN and 8.6 kN, respectively. The UDA and DA model failed at a total applied load of 37.2 kN and 50.8 kN, respectively.

3 Non-linear finite element models

This section describes the FE-models, calibrated using data obtained from the scale model tests. The calibrated variables were later used as mean values for the random variables in the PFEA (described in Sect. 4). Only the buttress mortar material parameters (see Sect. 3.1.1): modulus of elasticity, tensile strength, compressive strength, and fracture energy were assigned as random variables. The software used for the analysis was ATENA 2D V5. The geometry, interface locations, point load locations, monitor for crest horizontal displacement, and linear spring support locations of the UDA FE-model are depicted in Fig. 4. Note that only the interface geometry differs between the FE-models of UDA, DA, and UA, apart from the material parameters.

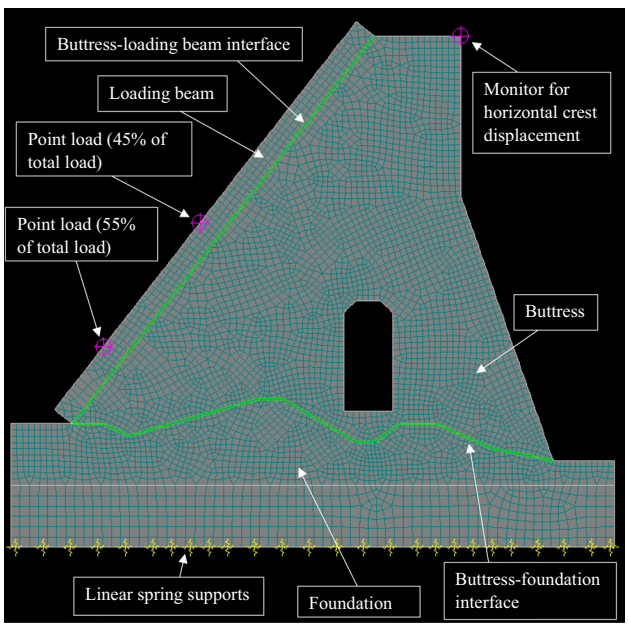

Fig. 4 FE-model of UDA

3.1 Material models

3.1.1 Buttress mortar

The mortar used in the buttress in the scale model tests by Sas et al. [19] was modelled by a fracture plastic model, with input material parameters shown for each model in Table 1. The modulus of elasticity, tensile strength, compressive strength, and the plastic strain at peak stress was taken from the cube samples experimentally tested by Sas et al. [19]. The fracture energies, G_f, of the buttress mortar mixes were not tested by the authors. Findings by Schneemeyer et al. [35] showed that low tensile strength mortars can have significantly lower fracture energy than regular concrete. As the aggregate sizes in the mix design for the scale models of the buttress were small (0–4 mm), the fracture energy was assumed to be unrepresentable by formulae presented in standard reference texts (e.g., MC2010 [36]). The fracture energy was instead approximated using a best-fit regression model (Eq. 1), presented by Pan et al. [37], for the relationship between fracture energy and maximum aggregate size, d_{max}. It was assumed to give representative results as the buttress mortar mix was comparable, in mix composition, to the concrete mixes used for the best fit regression.

$$G_f = 0.36 \times {d_{max}}^{1.69} [\mathrm{N/m}] \quad (1)$$

3.1.2 Interface, buttress-foundation

The interface between the buttresses and corresponding foundations was modelled using the interface model in ATENA 2D, which is based on the linear Mohr–Coulomb failure criterion with tension cut off [38]. As rubber spray paint was used to prevent bonding between the buttresses and their foundations in the experiments of Sas et al. [19], a value of zero was given to the cohesion of the interface as it proved to be numerically stable. Tilt table tests were performed on three cube samples for each buttress model in the experimental tests by Sas et al. [19], and the mean value for the individual buttress mix was used to estimate the basic friction angles of models UDA and DA. The mean value for the UA scale model's three cube samples was 36.1°. However, in the calibration of the UA FE-model, a friction angle of 37.8° provided better estimates of the failure load in preliminary simulations. Thus, 37.8°, which was within the range of measured basic friction angles of all the scale model's cube samples (33–39°), was applied in further FE analysis of the UA model. Interface stiffnesses and friction coefficients used in the FE-models in the study presented here are shown in Table 2.

The minimal normal or minimal tangential stiffnesses (${K_{nn}}^{MIN}$, ${K_{tt}}^{MIN}$) are the stiffness of the interface in its open state, i.e., when there is no contact between the adjoining elements. These parameters are required for numerical stability, and Červenka et al. [38] recommend use of one thousandth of the closed state stiffness as the minimum stiffness.

Table 1 Material parameters used in the FE-models

Concrete parameter	UDA	UA	DA
Modulus of elasticity, E [MPa]	8875	7300	5720
Tensile strength, f_t [MPa]	0.72	0.71	0.73
Compressive strength, f_c [MPa]	9.9	9.34	9.03
Plastic strain at strength f_c, ε_{CP} [–]	1.63×10^{-3}	9.67×10^{-4}	9.67×10^{-4}
Specific material weight, ρ [kN/m^3]	15.2	18.3	17.4
Reduction of compressive strength due to cracks, ${r_c}^{lim}$ [–]	0.8	0.8	0.8
Crack shear stiffening factor, S_F [–]	20	20	20
Poisson's ratio, ν [–]	0.2	0.2	0.2
Fracture energy, G_f [N/m]	3.75	3.75	3.75
Critical compressive displacement, w_d [m]	-5×10^{-4}	-5×10^{-4}	-5×10^{-4}

Table 2 Interface stiffnesses and their friction coefficients

Interface parameter	UDA	UA	DA
Normal stiffness, K_{nn} [MN/m^3]	4.4×10^6	3.7×10^6	2.9×10^6
Tangential stiffness, K_{tt} [MN/m^3]	2.8×10^6	1.5×10^6	1.2×10^6
Friction angle [°]	35.6	37.9	35.6
Friction coefficient [–]	0.716	0.775	0.716
Minimal normal stiffness, ${K_{nn}}^{MIN}$ [MN/m^3]	4.4×10^3	3.7×10^3	2.9×10^3
Minimal tangential stiffness, ${K_{tt}}^{MIN}$ [MN/m^3]	2.8×10^3	1.5×10^3	1.2×10^3

3.1.3 Loading beam

In the scale model tests by Sas et al. [19] hydraulic jacks applied loads through a loading beam (HEA 100). In the FE-models, the loading beam was represented by plane stress elements corresponding to the bending stiffness of a HEA 100 beam. A linear elastic material model was used for the loading beam, with an elastic modulus equal to 200 GPa.

3.1.4 Interface, loading beam-buttress

To connect the loading beam elements to the elements composing the buttress, an interface was implemented. In the experimental tests, this interface was an insulating material with unknown stiffness and friction. Therefore, the stiffness and friction angle of this interface were chosen based on optical strain measurements and tests of the behavior of the FE-models for different parameter values. For the numerical analyses, the friction coefficient was estimated to be 0.85 whereas the selected values for the normal and tangential stiffness of the interface were 638 MN/m^3 and 400 MN/m^3, respectively. The cohesion and tensile strength were 1 MPa and 0.1 MPa, respectively. Non-zero cohesion was required to keep the beam and pillar together in addition to increasing the numerical stability of the model.

3.1.5 Foundation

The foundation was modelled using a fracture plastic constitutive model with material parameters representative of C30/37 concrete as specified in the relevant Eurocode [34]. Reinforcement was not included in the foundation as preliminary analyses concluded that the stresses in the foundation were not exceeding its material strength.

3.2 Loads

Three load types were needed in the FE-models to account for all loads acting on the scale models. The loads, which had to be included, were the supports, self-weight, and point loads representing the hydraulic jacks.

3.2.1 Supports

Sas et al. [19] mentioned that in the scale model tests a gypsum layer was used to level the foundation and steel yokes were used to restrain the foundation laterally and anchor it vertically to the strong floor. To account for the stiffness of the fixing system, linear springs were used in the FE-models as boundary conditions (a spring stiffnesses of 1123 MPa in the horizontal direction and 151 MPa in the vertical direction, determined from DIC measurements of fixed points in the foundation).

3.2.2 Self-weight

The self-weight of the model was implemented using the load type 'body force' in which ATENA calculates the volume of each element in the mesh and applies an equivalent load to the element nodes based on the material model densities [38]. Thus, a realistic stress distribution in the model and buttress-foundation interface from the self-weight is given.

3.2.3 Point loads

Loads from the hydraulic jacks, used to simulate the hydrostatic pressure in the scale model tests, were implemented in the FE-models as point loads. The location and inclination of these point loads coincided with those of the hydraulic jacks along the loading beam in the scale model tests by Sas et al. [19]. These loads were increased until failure of the model.

4 Random variables

The variables assumed to have the most impact on the results from the scale model tests and therefore, chosen as random variables, were the modulus of elasticity, tensile strength, compressive strength, and fracture energy.

The variables were randomized in ATENA 2D's probabilistic module, FREET, which randomizes variables according to chosen distributions and coefficients of variation (COV) and assigns them to new copies of the base model. Relatively few simulations for each FE-model were sought due to the computational time required. Therefore, Latin hypercube sampling (LHS) was chosen as the sampling technique as Vořechovský [39] showed that LHS can rapidly reach convergence for a number of functions with relatively small sample sizes. This also enabled coverage of wide ranges of material parameter values.

Regarding the probability distribution functions used, a lognormal distribution was used for the compressive strength, f_c, as recommended by Silvestri et al. [40] and Westberg Wilde and Johansson [41]. Similarly, the modulus of elasticity, E, is highly correlated to the compressive strength [42], so a lognormal distribution was used for this variable. The Weibull distribution was used for the tensile strength (f_t) and fracture energy (G_f). The COVs were based on data presented by Strauss et al. [43]. The COVs and distributions used for the random variables are presented in Table 3 together with the corresponding mean values (which are also shown in Table 1).

Table 3 Randomized material parameters with their COVs, distributions, and mean values

Random variable	COV	Distribution	Mean values		
			UDA	UA	DA
Modulus of elasticity, E [MPa]	0.15	Lognormal	8875	7300	5720
Tensile strength, f_t [MPa]	0.18	Weibull	0.72	0.71	0.73
Compressive strength, f_c [MPa]	0.1	Lognormal	9.90	9.34	9.03
Fracture energy, G_f [N/m]	0.2	Weibull	3.75	3.75	3.75

The correlation matrix imposed on the randomization is based recommendations by Havlásek and Pukl [44] and is shown in Table 4.

Sample size was chosen by iteratively increasing samples until the spearman rank correlation for the parameters showed signs of convergence. With a sample size of 64 the resulting correlations were only slightly different from those obtained with a sample size of 32, so a sample size of 64 was considered satisfactory for purposes of this study.

5 Results and discussion

Results are presented in terms of load–displacement diagrams and scatterplots of the capacity vs. the individual parameter values. The parameters' influences on the total applied load (i.e., load capacity) were determined using Spearman's rank correlations and are summarized in Table 5. Spearman rank correlations were calculated for the maximum applied load and random variables for the UDA and DA models, but at a load resulting in a horizontal displacement of 0.4 mm at the crest for the UA model. A general remark regarding the numerical analyses is that they were good at simulating the behavior of the scale models in the experimental tests. No other type of failure than that shown in the experimental tests was observed, indicating that the same failure would occur even with differing material parameters.

The horizontal part of the presented load displacement diagrams (see Figs. 5, 11, and 17) indicates that both scale models and FEA models failed. This is indicated by the large displacement with no increase in load carrying capacity. At that point, the FE-models start to diverge slightly as they do not find a solution with less than 1% error margin. This part of the individual model's load–displacement diagram is, however, kept in the diagrams due to greater visibility of the maximum load.

Table 4 Correlation matrix for randomized material parameters

	E	f_t	f_c	G_f
E	1	0.6	0.9	0.5
f_t	0.6	1	0.6	0.9
f_c	0.9	0.6	1	0.6
G_f	0.5	0.9	0.6	1

Table 5 Spearman rank correlations for the randomized variables and applied load for each model simulation

Randomized variable	UDA	DA	UA*
Modulus of elasticity, E	0.577	0.785	0.998
Tensile strength, f_t	0.965	0.940	0.603
Compressive strength, f_c	0.662	0.831	0.915
Fracture energy, G_f	0.891	0.905	0.548

*For the applied load at a crest horizontal displacement of 0.4 mm

5.1 Model with the upstream and downstream asperity (UDA)

In eight simulations of this model, there were numerical errors and issues with convergence. These were neglected in the following presented results. Figure 5 displays the combined load–displacement diagram for all the UDA FEA models. The load displacement diagram obtained from the scale model test conducted by Sas et al. [19] is also presented in the figure.

Figure 5 shows that the load displacement curve from the scale model tests lies within the range of the maximum and minimum capacity of the numerical simulations. The average maximum applicable load for the numerical simulations was 35.6 kN (with a median of 36.1 kN), which correlates well with the experimental results of 37.2 kN. As previously mentioned, no other type of failure was seen in the numerical analyses even at the far ends of the material spectra.

Elements containing cracks at divergence in simulations of the UDA FEA model are the darker elements in Fig. 6a. Note that Fig. 6a only shows elements containing cracks and not crack widths. Small differences in crack widths and elements containing cracks between simulations were seen, but nothing indicative of another type of failure. Principal maximum strains of the same load step are shown in Fig. 6b. Strains from the DIC measurements of the UDA scale model tests [19] are shown in Fig. 6c for comparison with the FEA simulation.

Comparing the elements containing cracks and strains from the FEA with the DIC strain measurements from the scale model tests, it is apparent that the FE-model successfully captures the cracking pattern and failure observed in the scale model tests by Sas et al. [19]. Post-processing of

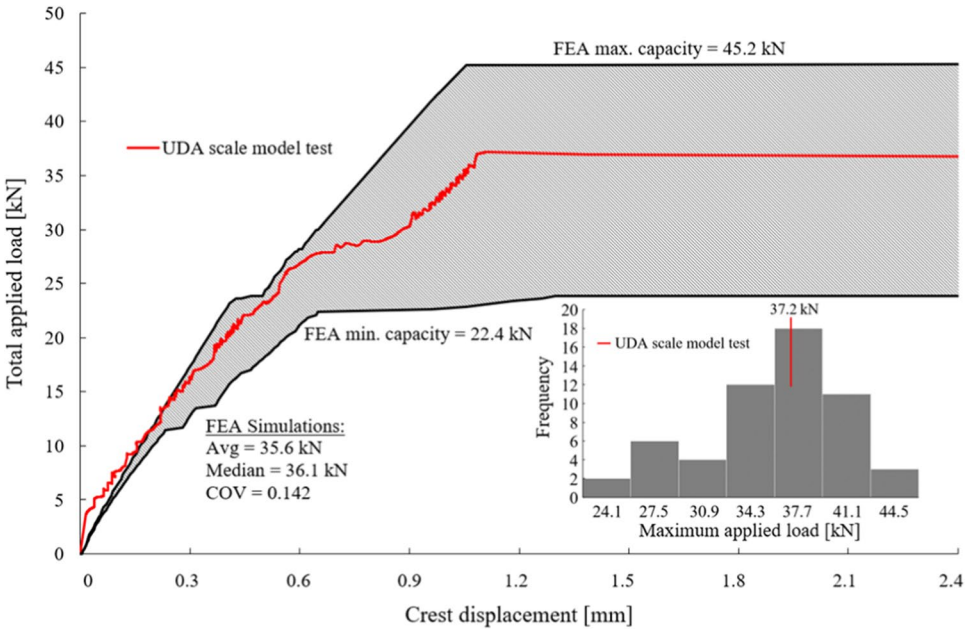

Fig. 5 Load [kN] displacement [mm] diagram for scale model test and results from FEA simulations of the UDA model

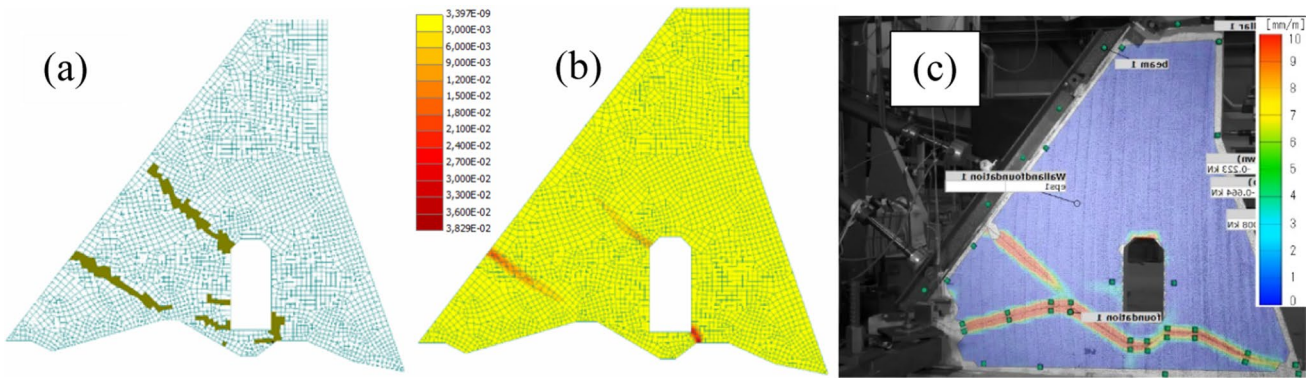

Fig. 6 **a** Elements containing cracks in the FEA simulation of UDA at divergence. **b** Strains in the FEA simulation of UDA at divergence. **c** DIC strain measurements at the point of failure in scale model tests [19], reproduced under the terms of the Creative Commons Attribution (CC BY 4.0) license

the UDA FE-models revealed a common pattern leading up to the failure. Firstly, the crack in the bottom right of the doorway emerges and widens, allowing for some slippage along the interface. The buttress then interlocks with the back asperity causing it to rotate around the fulcrum next to the back asperity. This rotation results in a gap emerging at the front end of the buttress, leading to the buttress being supported solely by interlocking with the back asperity. At this point, the front end of the buttress acts similarly to a corbel and fails when the diagonally spanning crack from the front asperity emerges. Judging from the failure mechanism observed, the doorway generates a weak zone in the buttress body as it is located near the highly stressed downstream asperity.

The failure implies that the tensile strength of the buttress material will affect the capacity as the failure occurs similarly to when the tensile strength is exceeded by the principal maximum stress at the front of the buttress. This reasoning is further supported by the correlation between the individual parameters and the maximum applicable load (presented in Table 5). These correlations do not include the simulations which were deemed to be affected by divergence from numerical errors.

The correlations show that the applied load in the FE-models is highly dependent on the tensile parameters of the buttress material, especially the tensile strength. However, comparing the correlation matrix imposed on the random variables (Table 4) with the Spearman rank correlation

(Table 5) it can be seen that there is high similarity between the individual material parameters correlation to the tensile strength, and the Spearman rank correlation for the total applied load. This implies that the critical parameter for the capacity is only the tensile strength whereas the high Spearman rank correlation for the other material parameters stem from the correlation to the tensile strength. This is manifested in the common pattern in scatterplots of the randomized variables' values versus the corresponding tensile strength and randomized variables' values versus total applied load. Such scatterplot of the modulus of elasticity, tensile strength, compressive strength, and fracture energy are shown in Figs. 7, 8, 9, and 10, respectively. FEA simulations considered to have diverged prematurely due to numerical errors were omitted in the scatterplots.

The scatterplots show that the tensile strength vs. applied load data points generated by the numerical simulations form an almost linear band, the dots and crosses form almost indistinguishable pattern and the groupings displayed in Figs. 7, 8, 9, and 10 are tighter when the parameters are highly correlated with the tensile strength.

Results of the numerical simulations of the UDA FE-model clearly indicate that the numerical model, and experimental tests performed by Sas et al. [19], were highly dependent on the tensile strength. In addition, no other failure mode was witnessed under a different tensile strength of the buttress material.

5.2 Model with the downstream asperity (DA)

For the simulations of the DA model, all FEA models converged to the extent where the same failure could be seen and there was no clear evidence of numerical errors such that those occurred in some FEA simulations of the UDA model. Figure 11 portrays the combined load–displacement diagram for all the DA simulations, and also shows the load displacement diagram from the scale model test conducted by Sas et al. [19].

Figure 11 shows that the elastic branch of the load vs displacement curve had steeper inclination in the scale model

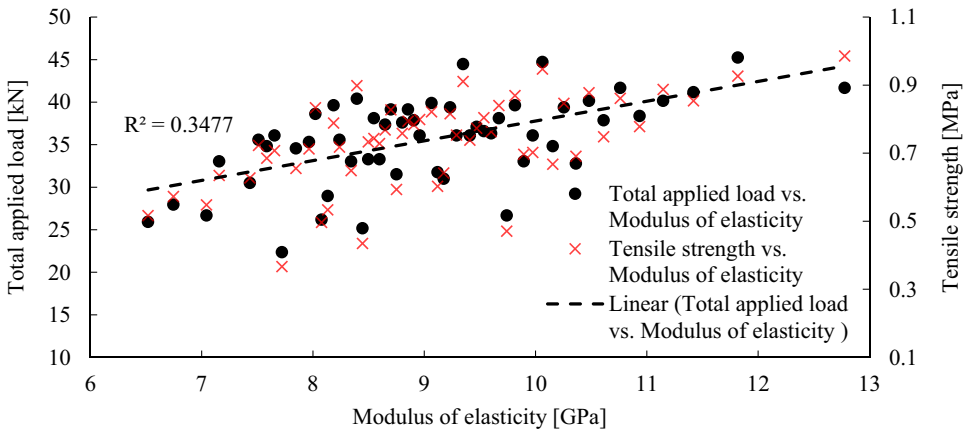

Fig. 7 Total applied load [kN] vs. Modulus of elasticity [MPa] and Tensile strength [MPa] vs. Modulus of elasticity for the UDA model simulations

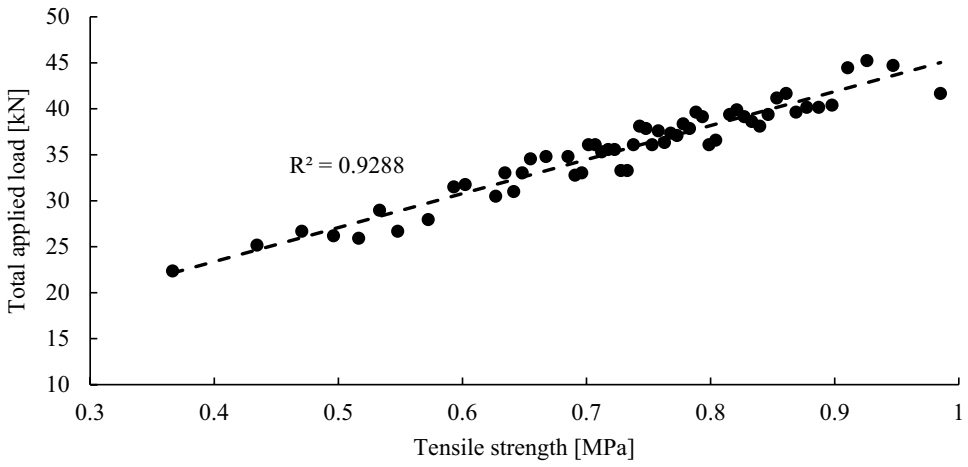

Fig. 8 Total applied load [kN] vs. Tensile strength [MPa] for the UDA model simulations

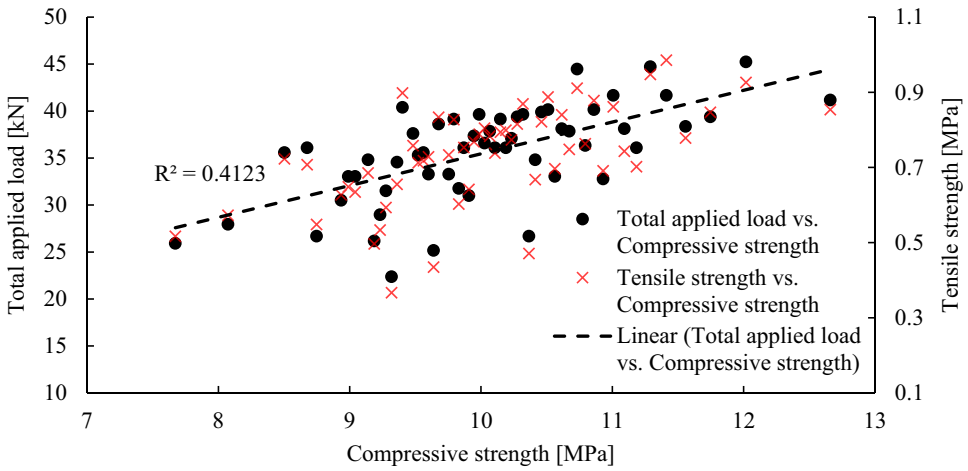

Fig. 9 Total applied load [kN] vs. Compressive strength [MPa] and Tensile strength [MPa] vs Compressive strength vs. for the UDA model simulations

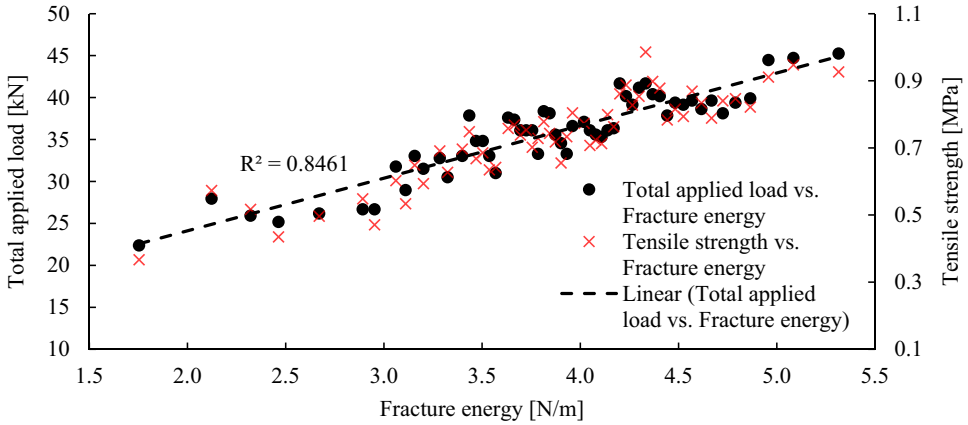

Fig. 10 Total applied load [kN] vs. Fracture energy [N/m] and Tensile strength vs. Fracture energy [N/m] for the UDA model simulations

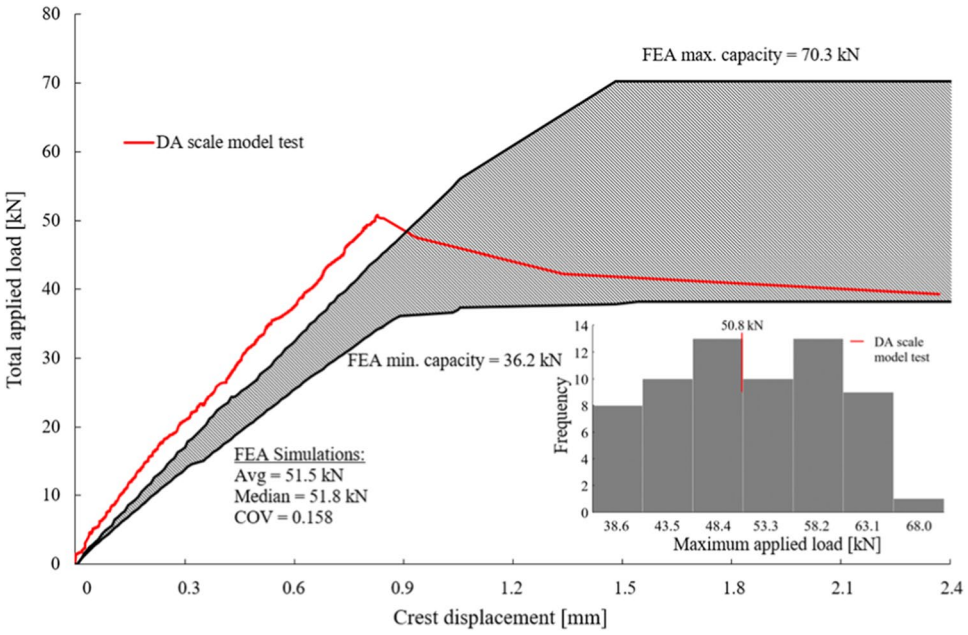

Fig. 11 Load [kN] displacement [mm] diagram for scale model test and results from FEA simulations of the DA model

tests than in the FEA simulations. This is attributed to the stiffness of the implemented spring supports being slightly lower in the FE-model than that of the gypsum board in the experimental tests. Preliminary FEA simulations with rigid supports instead of spring supports generated noticeably greater inclination of the load–displacement curve in the elastic region than in the load–displacement diagram from the scale model tests. Although the spring stiffness affected the inclination of the elastic branch, the preliminary simulations with completely rigid supports showed that the difference in total applied load barely increased (by less than 5%) when using spring supports. The average maximum applicable load for the FE-simulations was 51.5 kN (a median of 51.8 kN) in contrast to 50.8 kN obtained from the scale model tests. It can further be seen that the maximum load applied on the scale model is enveloped by the maximum and minimum total applied loads of the FEA simulations.

The elements containing cracks in the DA FEA simulation are the darker elements in Fig. 12a. Strains from the DA FEA simulation and DIC measurements of the DA scale model tests [19] are shown in Fig. 12b and c, respectively. There were slight variations in crack sizes and patterns between the FEA simulations and scale model test, but not to an extent indicative of another type of failure.

Comparison of the DIC strain measurements and elements containing cracks and strains in the FEA simulation of the DA model show that the simulation accurately captures the failure in the experimental test.

Similar to the phenomena observed in the UDA FEA models, the process leading up to failure of the DA models is initiated by widening of the crack in the bottom right of the doorway. This allows for rotation of the buttress near the back asperity as it completely supports the load as interlocking occur, leading to no force transfer through the interface in front of the back asperity. The models start to have difficulties converging as the cracks left of the doorway appear and these difficulties are aggravated as the cracks widen. As in the UDA model, the failure seems to be governed by the tensile strength of the buttress material and is confirmed by the Spearman rank correlation (Table 5) for the individual parameters and the maximum applicable load.

The tensile strength and fracture energy seem to have high correlation with the maximum appliable load of the FE-model. High dependency can also be seen on the modulus of elasticity and compressive strength, which can be attributed to the correlation with the tensile strength in the randomization process. However, in contrast to the correlations for the UDA models, this is not the only cause of the high Spearman rank correlations of these parameters as they are significantly higher than the corresponding material parameter correlations (Table 4). The tensile strength reduction factor ATENA uses to account for biaxial failure becomes more influential as this is governed by the compressive-strength and stresses [38]. As higher minimum principal stresses are present in the DA model than in the UDA model, the compressive strength plays a larger role in the reduction factor and thus the results of, and Spearman rank correlations in, each DA model.

Scatterplots of the studied material parameters (modulus of elasticity, tensile strength, compressive strength, and fracture energy) vs. the maximum appliable load are presented in Figs. 13, 14, 15, and 16, respectively. No crosses showing the parameters' relationships with tensile strength are included in these scatterplots, unlike those of the UDA FEA simulations, as the common pattern of correlations with the tensile strength and maximum appliable load was not as evident for the DA FEA simulations.

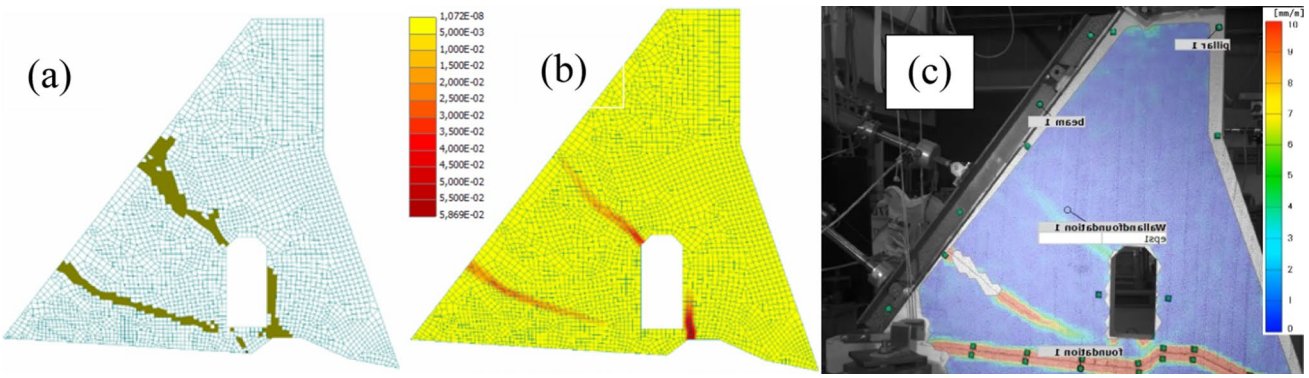

Fig. 12 **a** Elements containing cracks in the FEA simulation of DA at divergence. **b** Strains in the FEA simulation of DA at divergence. **c** DIC strain measurements at point of failure in scale model tests [19], reproduced under the terms of the Creative Commons Attribution (CC BY 4.0) license

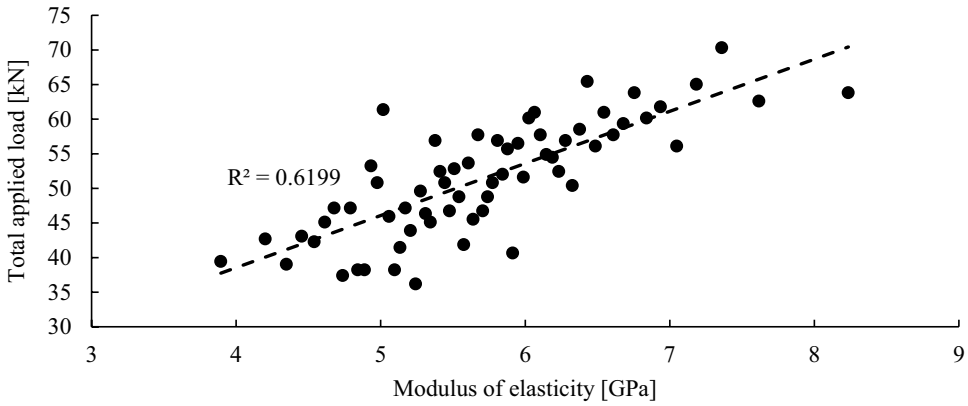

Fig. 13 Total applied load [kN] vs. Modulus of elasticity [MPa] for the DA model simulations

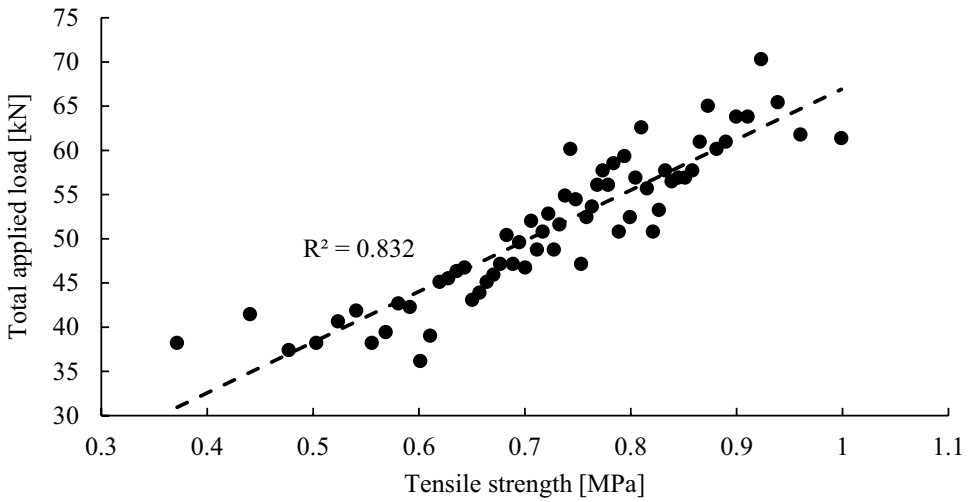

Fig. 14 Total applicable load [kN] vs. Tensile strength [MPa] for the DA model simulations

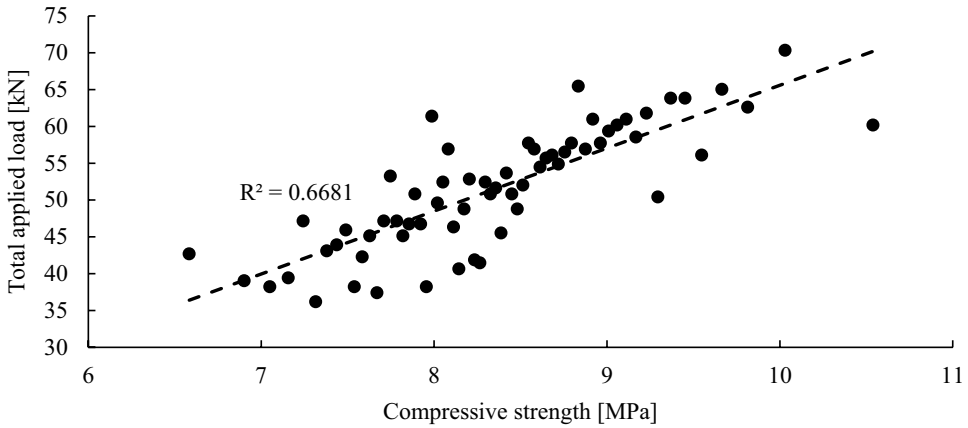

Fig. 15 Total applicable load [kN] vs. Compressive strength [MPa] for the DA model simulations

There is less scatter in the plots of values generated in the DA FEA simulations than in those of the UDA FEA simulations as the results have more dependence on each specific parameter rather than just the tensile strength. This implies that the load at which the buttress would fail could depend on any of the parameters, although the tensile strength may be the most influential. However, the failure mode would be independent of the material parameters as it was consistent for all simulations.

5.3 Model with the upstream asperity (UA)

In the scale model tests, the UA model slid along the interface without fracture in the buttress and this failure

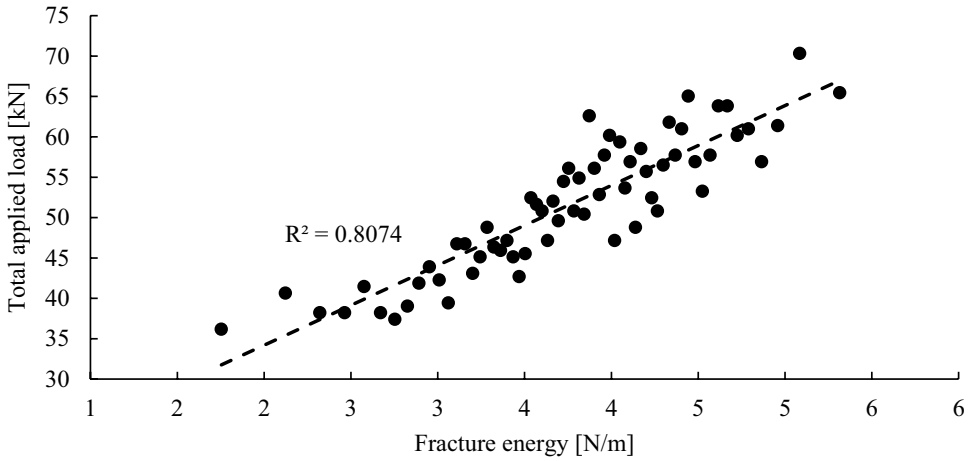

Fig. 16 Total applicable load [kN] vs. Fracture energy [N/m] for the DA model simulations

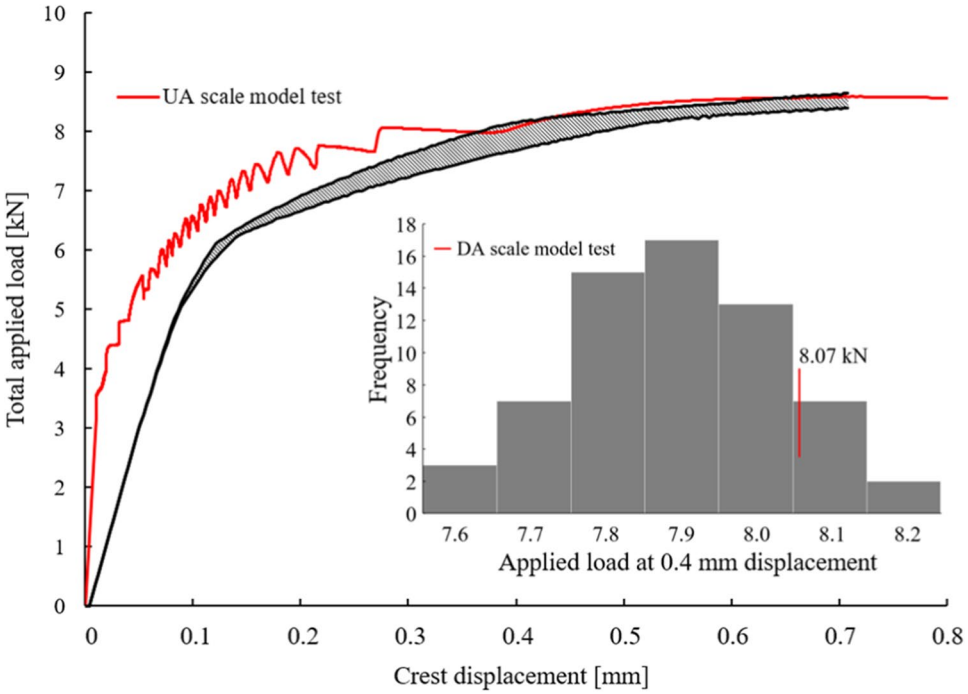

Fig. 17 Load [kN] displacement [mm] diagram for scale model test and results from FEA simulations of the UA model

mode was replicated in all the FEA simulations of the UA model. Running the UA FEA models, some convergence difficulties were encountered. The FEA models had difficulties converging past a horizontal crest displacement of 0.5 mm and rapidly diverged with no indication of numerical instability in the last load steps. The UA FEA simulations combined load displacement diagram is shown in Fig. 17. As the models had problems converging, the average, median, and COVs for the ultimate load are not presented in Fig. 17. The load displacement diagram from the scale model test conducted by Sas et al. [19] is also shown in the figure.

The initial part of the load–displacement curve obtained from the experimental tests has a steeper inclination than the numerical simulations. As in the DA models, this is likely caused by the stiffness of the supporting springs in the FEA models being lower than that of the gypsum board in the experimental tests. However, this does not seem to impact the total applied load in the simulations since they converge toward the load displacement curve for the scale model test. The jumps in the scale model tests by Sas et al. [19] are thought to be caused by the buttress slipping incrementally along the buttress-foundation interface.

Figure 18 depicts horizontal displacement of the FEA simulation of the UA model as it slides along the interface

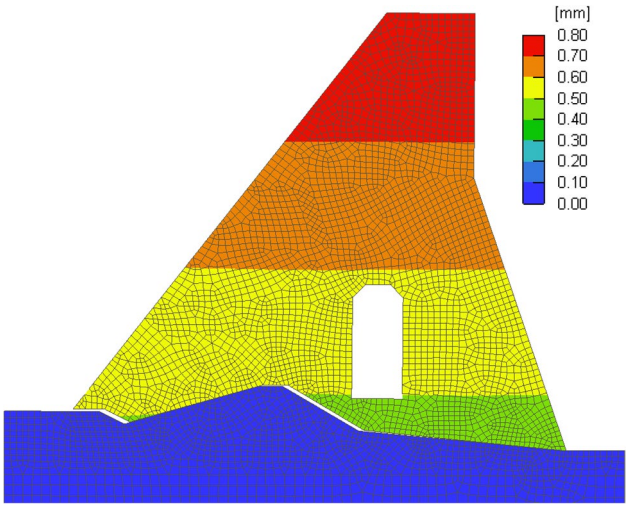

Fig. 18 Horizontal displacement [mm] at divergence of the FEA simulation of the UA model

in later stages of the analysis. Note that the scale of the displacements is exaggerated.

Miniscule cracks (less than 1 μm wide) were present in the sharp corners of the mesh in the simulations of the UA model. However, these cracks did not propagate after their initiation during early stages of the simulations. Therefore, the randomized material parameters do not have an impact on the total applied load (i.e., capacity) in the FEA models. This is supported by the tight grouping in Fig. 17. Also, as the FEA simulations had convergence issues, calculating the parameters' Spearman rank correlation for the maximum applied load would only indicate which parameter was most important for convergence. Therefore, Spearman rank correlations were calculated for the total applied load at the load step where the crest's horizontal displacement was 0.4 mm, instead of at the last converged load step (as for the FEA simulations of the UDA and DA FEA models). Thus, the presented correlations for the UA FEA models indicate which parameter is the most influential for the load required to cause a crest displacement of 0.4 mm. The value of 0.4 mm was chosen as all FEA simulations of UA were able to converge to this displacement. The calculated Spearman rank correlations are shown in Table 5.

The Spearman rank correlations for the UA FEA simulations indicate almost complete dependence on the modulus of elasticity. While the other Spearman rank correlations of the randomized variables are almost equal to their correlations with the modulus of elasticity (Table 4). Values of the modulus of elasticity vs. the total applied load at 0.4 mm of crest horizontal displacement are shown in Fig. 19, and values of the other randomized variables (tensile strength, compressive strength, and fracture energy) vs. modulus of elasticity and total applied load are shown in Figs. 20, 21, and 22, respectively.

A linear relationship can be seen in Fig. 19, which shows the modulus of elasticity vs. the applied load at a crest displacement of 0.4 mm. Patterns are similar for the other randomized variables, as shown by similarity of the of crosses and dots in Figs. 19, 20, and 21, implying that they have no significant impact on the applied load. This suggests failure in the buttress in unlikely for the UA models (and dams with similarly low inclined asperities near the upstream face), even for low values of the material strengths.

Although not affecting the load capacity of the models, the modulus of elasticity seems to have a considerable impact on the crest horizontal displacement as seen from the load–displacement diagram (Fig. 17). The discrepancy in the horizontal crest displacement between the FE-models with the maximum and minimum modulus of elasticity increased with load and becomes significant near the failure load.

6 Concluding remarks

The aim of this study was to show how probabilistic finite element method can be used to predict complex failure mechanism in concrete dams using data obtained from previous scale model tests of a buttress section in a real dam. The

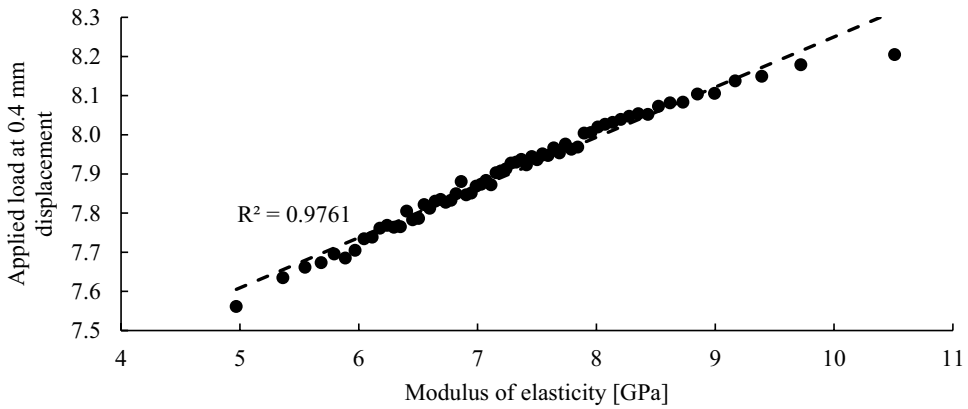

Fig. 19 Applied load [kN] at 0.4 mm of crest displacement vs. Modulus of elasticity [MPa] for the UA model simulations

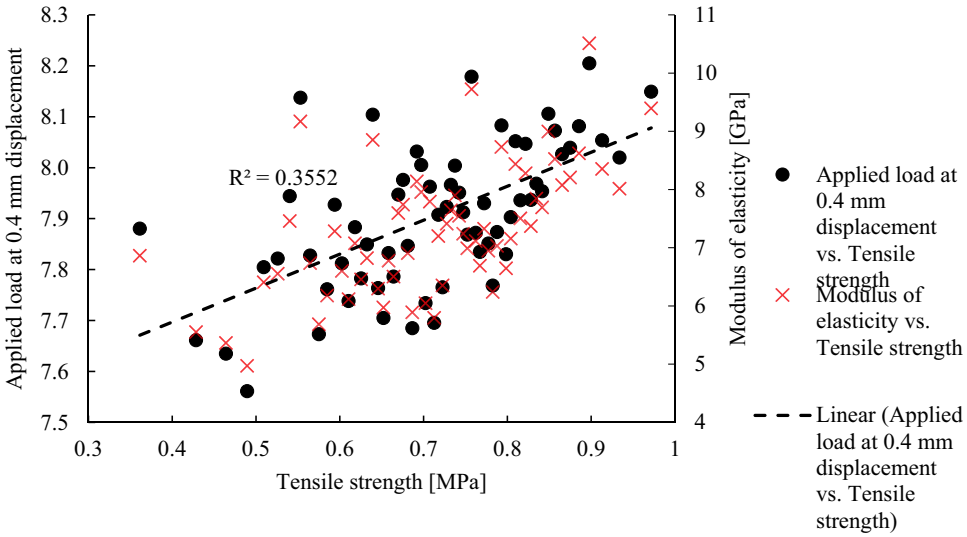

Fig. 20 Applied load [kN] at 0.4 mm of crest displacement vs. Tensile strength [MPa] and Modulus of elasticity [MPa] vs. Tensile strength for the UA model simulations

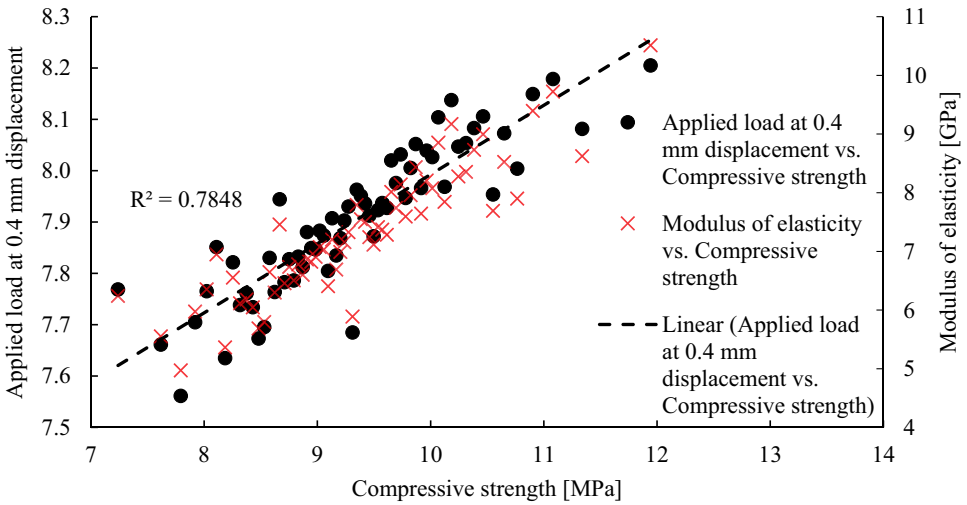

Fig. 21 Applied load [kN] at 0.4 mm of crest displacement vs. Compressive strength [MPa] and Modulus of elasticity [MPa] vs. Compressive strength for the UA model simulations

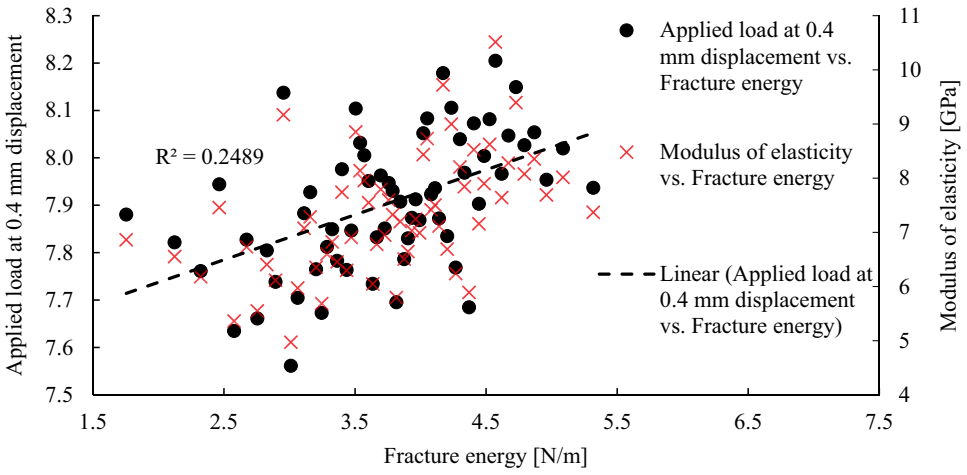

Fig. 22 Applied load [kN] at 0.4 mm of crest displacement vs. Fracture energy [N/m] and Modulus of elasticity [MPa] vs. Fracture energy for the UA model simulations

PFEA was performed on reduced scale models, but these results and the method is not limited to any scale and can be extended to full scale concrete dams to better understand its behavior and capacity.

The models that included the large-scale asperity, with the steeper inclination close to the downstream side, failed by rupture of the dam body as interlocking occurred between the dam body and foundation. As expected, these models displayed strong correlations between the material parameters, used as random variables (especially the tensile strength), and the ultimate capacity. The same failure mode occurred for all simulations even with large differences between the maximum and minimum material strengths. This is possibly explained by the fact that the interlocking, which marked the initiation of the seen failures, was not influenced by the randomized material parameters. Failure to consider the large-scale asperities in analytical assessment would suggest that the studied buttresses would slide along the interface and that the capacity would be governed by the shear strength of the interface. However, based on the results from this study, a real dam with one or more steeply inclined large-scale asperities could likely fail due to stresses exceeding the material strengths in either the foundation or dam.

In the UA (upstream asperity) models, containing the larger asperity near the upstream side with lower inclination, there was little dependency on the material parameters in the dam body for the ultimate capacity. The buttress material stayed in the elastic stage throughout the whole simulation and the models repeatedly failed by sliding along the rock–concrete interface, even for large variations of the buttress material's strength parameters. The load capacities of these models were, therefore, independent of the randomized material parameters in the buttress and instead, likely relies on the rock–concrete interface's shear strength parameters. However, the modulus of elasticity of the buttress material had considerable impact on the crest horizontal displacement near failure.

Failures related to dam foundations were not studied. However, the FEA approach adopted in this study could prove useful in determining if such failures could be governing as stress concentrations were observed in the post-processing of the models which contained the downstream asperity. The presence of such stress concentrations could imply that failure in the foundation is governing, instead of failure in the dam or rock–concrete interface.

Neither the material parameters that were randomized nor the failure mechanism seen in this study are commonly considered to be governing in assessment methods that are often used. This discovery of a material parameter dependency for certain types of failures, where no analytical method exists, highlights the need for more refined methods to assess concrete dams, as the capacity and failure mechanism may otherwise be misjudged.

As demonstrated in this paper, the influence of the dam's material properties on the capacity of the dam is heavily dependent on the geometrical variation in the rock–concrete interface. Further research is required to evaluate how the failure mode for a dam with significant geometrical variations at the interface is affected by parameters such as friction angle and cohesion. In addition, due to the large variability of the geometry of the rock–concrete interface, identification of the cases in which interlocking can be expected is of high interest. A similar issue relates to the geometry of discontinuities in the dam´s body (e.g., doorways, galleries, etc.), that can influence the overall capacity of the structure and its associated failure mode.

Author contributions AU: data collection, data analysis, data preparation, methodology, writing original draft, and review. JG-L: supervision, manuscript review and editing. OD: supervision, manuscript review and editing. DB: manuscript review and editing. MWW: supervision, manuscript review and editing. FJ: supervision, manuscript review and editing. GS: funding acquisition, supervision, manuscript review and editing.

Funding Open access funding provided by Lulea University of Technology. The authors are grateful to the various funding agencies, namely, the 'Stable dams' project funded by the Research Council of Norway (Grant No. 244029), FORMAS (Grant No. 2019–01236), and Swedish Hydropower Center (SVC) (Grant VKU14169) that supported the development of the research presented in this article.

Data availability Data will be made available upon reasonable request.

Declarations

Conflict of interest The authors declare that they have no known competing financial interests or personal relationships that would influence the work reported in this paper.

Ethical approval This submission nor parts of its content has been submitted to any journal for simultaneous publication nor has it already been published elsewhere in any language or form. The submission contains the study in full and there are no concurrent or secondary publications. Results are presented honestly without falsification and fabrication with the intent of misleading readers. Proper acknowledgements are given, and the presented data, text, and theories are the authors' own. No animals and human test subjects were used in this study. All the authors of the submission consent to the publication of the article and raw data will be provide upon request.

References

1. USACE. Gravity dam design. US Army Corps of Engineers; 1995.
2. CFGB. Small dams—Guidelines for Design, Construction and Monitoring. French Committee on Large Dams; 2002.
3. CDA. Dam Safety Guidelines 2007. Canadian Dam Association; 2013.
4. ANCOLD. Guidelines on design criteria for concrete gravity dams. Australian National Committee on Large Dams; 1991.
5. IS. Criteria for design of solid gravity dams. IS: 6512-2003. 2003. Report No.: IS 6512.
6. NVE. Retningslinjer for betongdammer til § 4.8 i forskrift om sikkerhet og tilsyn med vassdragsanlegg. Norges vassdrags og-energidirektorat, Directorate NWRaE; 2005. (**in Norwegian**).
7. FERC. Engineering Guidelines for the Evaluation of Hydropower Projects: 3 Federal Energy Regulatory Commission; 2016.
8. Patton FD. Multiple modes of shear failure in rock. Proceedings of the 1st international Congress of Rock Mechanics: International Society for Rock Mechanics; 1966.
9. Grasselli G. Shear strength of rock joints based on quantified surface description. Lausanne: École polytechnique fédérale de Lausanne; 2001.
10. Asadi MS, Rasouli V, Barla G. A laboratory shear cell used for simulation of shear strength and asperity degradation of rough rock fractures. Rock Mech Rock Eng. 2013;46(4):683–99.
11. Gravel C, Moradian OZ, Fathi A, Ballivy G, Quirion M. In Situ Shear Testing of Simulated Dam Concrete-Rock Interfaces. 2015.
12. Ladanyi B, Archambault G. Simulation of shear behavior of a jointed rock mass. Proceedings of the 11th Symposium on Rock Mechanics. 1969;1.
13. Barton N, Choubey V. The shear strength of rock joints in theory and practice. Rock Mech. 1977;10(1):1–54.
14. Grasselli G. Manuel rocha medal recipient shear strength of rock joints based on quantified surface description. Rock Mech Rock Eng. 2006;39(4):295.
15. Johansson F, Stille H. A conceptual model for the peak shear strength of fresh and unweathered rock joints. Int J Rock Mech Min Sci. 2014;69:31–8.
16. Zhang X, Jiang Q, Chen N, Wei W, Feng X. Laboratory investigation on shear behavior of rock joints and a new peak shear strength criterion. Rock Mech Rock Eng. 2016;49(9):3495–512.
17. Ríos-Bayona F, Johansson F, Mas-Ivars D. Prediction of peak shear strength of natural, unfilled rock joints accounting for matedness based on measured aperture. Rock Mech Rock Eng. 2021;54(3):1533–50.
18. Chen Y, Lin H, Li S, Cao R, Yong W, Wang Y, et al. Shear expression derivation and parameter evaluation of Hoek-Brown criterion. Archiv Civil Mech Eng. 2022;22(2):77.
19. Sas G, Popescu C, Bista D, Seger A, Arntsen B, Johansson F, et al. Influence of large-scale asperities on the shear strength of concrete-rock interface of small buttress dams. Eng Struct. 2021;245:112952.
20. Hencher SR, Richards LR. Assessing the shear strength of rock discontinuities at laboratory and field scales. Rock Mech Rock Eng. 2015;48(3):883–905.
21. Johansson F. Shear Strength of Unfilled and Rough Rock Joints in Sliding Stability Analyses of Concrete Dams. Diva: Kungliga Tekniska Högskolan; 2009.
22. Liahagen SA. Stabilitet av betongdammer - Ruhetens påvirkning på skjærkapasiteten mellom betong og berg: Norges teknisk-naturvitenskapelige universitet; 2012.
23. Bista D, Sas G, Johansson F, Lia L. Influence of location of large-scale asperity on shear strength of concrete-rock interface under eccentric load. J Rock Mech Geotech Eng. 2020;12(3):449–60.
24. Harris HG, Sabnis GM. Structural modelling and experimental techniques. 2nd ed. Boca Raton: CRC Press; 1999.
25. Barpi F, Valente S. Numerical simulation of prenotched gravity dam models. J Eng Mech. 2000;126(6):611–9.
26. Liu J, Feng X-T, Ding X-L, Zhang J, Yue D-M. Stability assessment of the Three-Gorges Dam foundation, China, using physical and numerical modeling—Part I: physical model tests. Int J Rock Mech Min Sci. 2003;40(5):609–31.
27. Harris DW, Travers F. Investigation of the Failure Modes of Concrete Dams - Physical Model Tests. U.S. Department of the Interior Bureau of Reclamation; 2006. Contract No.: DSO-06-03.
28. Zhu HH, Yin J-H, Dong J-H, Zhang L. Physical modelling of sliding failure of concrete gravity dam under overloading condition. Geomechanics and Engineering. 2010;2:89–106.
29. Chen Y, Zhang L, Yang B, Dong J, Chen J. Geomechanical model test on dam stability and application to Jinping High arch dam. Int J Rock Mech Min Sci. 2015;76:1–9.
30. Madier D. Practical Finite Element Analysis - For Mechanical Engineers. 1st ed. Canada: FEA Academy; 2020.
31. Novák D, Teplý B, Keršner Z, Vořechovský M. Freet program documentation. Brno: Czech Republic; 2002.
32. Xia C-C, Tang Z-C, Xiao W-M, Song Y-L. new peak shear strength criterion of rock joints based on quantified surface description. Rock Mech Rock Eng. 2014;47(2):387–400.
33. Buckingham E. On physically similar systems; illustrations of the use of dimensional equations. Phys Rev. 1914;4(4):345–76.
34. European Committee for Standardization. EN 1992-1-1, Eurocode 2: Design of concrete structures - Part 1-1: General rules and rules for buildings. 2004.
35. Schneemayer A, Schranz C, Kolbitsch A, Tschegg EK. Fracture-mechanical properties of mortar-to-brick interfaces. J Mater Civ Eng. 2014;26(9):04014060.
36. Fédération internationale du béton F. fib Model Code for Concrete Structures 2010. Berlin, Germany; 2013.
37. Pan T, Linbings W, Tutumluer E. Experimental investigation of aggregate-mortar interface affecting the early fracture toughness of portland cement concrete. International Journal of Pavement Research and Technology. 2011;4:168.
38. Červenka V, Jendele L, Červenka J. Atena program documentation—Part 1. Prague: Czech Republic; 2020.
39. Vorechovsky M, editor Extension of sample size in Latin Hypercube Sampling with correlated variables. 4th International Workshop on Reliable Engineering Computing; 2010; Singapore2009.
40. Silvestri S, Gasparini G, Trombetti T, Ceccoli C, editors. Towards the identification of accurate probability distribution models for the compressive strength of concrete. The 14th World Conference on Earthquake Engineering, Beijing; 2008.
41. Westberg Wilde M, Johansson F. Probabilistic model code for concrete dams—Part I, Part II, Part III and example. Energiforsk.se; 2016. Contract No.: 2016:292.
42. Nematzadeh M, Naghipour M. Compressive strength and modulus of elasticity of freshly compressed concrete. Constr Build Mater. 2012;34:476–85.
43. Strauss A, Hoffmann S, Wan-Wendner R, Bergmeister K. Structural assessment and reliability analysis for existing engineering structures, applications for real structures. Struct Infrastruct Eng. 2009;5:277–86.
44. Havlásek P, Pukl R. Sara program documentation. Prague: Czech Republic; 2017.